Coupled Reactions of Condensation and Charge Transfer. 1. Formation of Olefin Dimer Ions in Reactions with Ionized Aromatics. Gas-Phase Studies

Michael Meot-Ner (Mautner),* Yezdi B. Pithawalla, Junling Gao, and M. Samy El-Shall*

Contribution from the Department of Chemistry, Virginia Commonwealth University, Richmond, Virginia 23284-2006

Received July 31, 1996[⊗]

Abstract: The toluene radical ion $C_6H_5CH_3^{\bullet+}$, generated by resonance two-photon ionization, does not react with a single isobutene molecule (*i*-C_4H_8) which has a significantly higher ionization potential ($\Delta IP = 0.42$ eV). However, a reaction is observed involving two *i*-C_4H_8 molecules, to form the dimer ion $C_8H_{16}^{\bullet+}$. A coupled reaction of dimer formation and charge transfer to the dimer is exothermic if the product is an ionized hexene with a low IP. Correspondingly, the observed nominal second-order rate coefficients, $(5-25) \times 10^{-12}$ cm^3 s^{-1}, are enhanced by a factor of $>10^5$ over the expected value for direct endothermic charge transfer. Pressure and concentration effects suggest a sequential mechanism that proceeds through a $C_6H_5CH_3^{\bullet+}$(*i*-C_4H_8) reactive π complex. The complex can isomerize to a nonreactive $CH_3C_6H_4$-*t*-$C_4H_9^{\bullet+}$ adduct, or react with a second *i*-C_4H_8 molecule to form a $C_6H_5CH_3^{\bullet+}$-(*i*-C_4H_8)$_2$ complex, in which the olefin molecules are activated by the aromatic ion. Similar reactions are observed in the benzene/propene system with a somewhat larger ΔIP of 0.48 eV, suggesting that the charge density on the olefin in the complex is still sufficient to activate it for nucleophilic attack. However, aromatic/olefin systems with $\Delta IP > 0.87$ eV show no olefin dimer formation. At low [*i*-C_4H_8] and [Ar] number densities, the rate of formation of $C_8H_{16}^{\bullet+}$ is proportional to [*i*-C_4H_8]^2[Ar]. The corresponding fourth-order rate coefficient shows a strong negative temperature coefficient with $k = 11 \times 10^{-42}$ cm^9 s^{-1} at 300 K and 2×10^{-42} cm^9 s^{-1} at 346 K, suggesting that the mechanism can be efficient in low-temperature industrial and interstellar environments. The direct formation of the dimer bypasses the monomer olefin cation and its consequent side-reactions, and directs the products selectively into radical ion polymerization. The products and energy relationships that apply in the gas phase are observed also in clusters.

Introduction

Ionic polymerization of olefins B can be initiated by ionization of the olefin by various mechanisms, including charge transfer from another radical cation $A^{\bullet+}$ to form $B^{\bullet+}$. In the gas phase, these reactions are efficient when the ionization potential (IP) of the olefin is comparable to or lower than that of A, and the reaction is exothermic.

In this paper, we examine reaction systems where the opposite is true, i.e., the ionization potential of the olefin is substantially higher than that of the aromatic initiator. This rules out direct charge transfer from $A^{\bullet+}$ to B. However, under favorable conditions, a reaction with the overall stoichiometry of reaction 1 can be then energetically favorable, if the product is the ion of a larger olefin whose IP is lower than that of **A**.

$$A^{\bullet+} + 2B \rightarrow B_2^{\bullet+} + A \qquad (1)$$

Since three-body collisions are improbable, reaction 1 requires a sequential mechanism, as will be discussed below. This mechanism directs the products selectively into the radical cation polymerization channel, and avoids side reactions that would result from reactions of the monomer olefin ion.

Reaction 1 constitutes a specific initiation mechanism, in addition to catalysis,[1−3] ionizing radiation[4,5] electrode processes,[1−3] or impact by metal atoms or ions that were reported recently.[6−8] The initiation mechanisms can be best isolated and studied in the gas phase or in clusters,[9−21] and the results then applied to the condensed phase. For example, our recent studies of the reactions of metal ions with isobutene have lead to a novel

[⊗] Abstract published in *Advance ACS Abstracts,* August 15, 1997.

(1) Kennedy, J. P.; Marechal, E. *Carbocationic Polymerization;* Wiley: John and Sons: New York, 1982.
(2) Goethals, E. S., Ed. *Cationic Polymerization and Related Processes;* Academic Press: New York, 1984.
(3) Ystenes, M. J. *Catalysis* **1991**, *129*, 383.
(4) Taylor, R. B.; Williams, F. *J. Am. Chem. Soc.* **1969**, *91*, 3728.
(5) Okamato, H.; Fueki, K.; Kuri, Z. *J. Phys. Chem.* **1967**, *71*, 3222.
(6) Vann, W.; Daly, G. M.; El-Shall, M. S. In *Laser Ablation in Materials Processing*: *Fundamentals and Applications;* Braren, B., Dubowski, J., Norton, D., Eds.; MRS Symposium Proceedings Series; 1993; Vol. 285, p 593. Vann, W.; El-Shall, M. S. *J. Am. Chem. Soc.* **1993**, *115*, 4385.
(7) Deakin, L.; Den Auwer, C.; Revol, J. F.; Andrews, M. P. *J. Am. Chem. Soc.* **1995**, *117*, 9916.
(8) El-Shall, M. S.; Slack, W. *Macromolecules* **1995**, *28*, 8546.
(9) El-Shall, M. S.; Marks, C. *J. Phys. Chem.* **1991**, *95*, 4932.
(10) El-Shall, M. S.; Schriver, K. E. *J. Chem. Phys.* **1991**, *95*, 3001.
(11) Coolbaugh, M. T.; Vaidyanathan, G.; Peifer, W. R.; Garvey, J. F. *J. Phys. Chem.* **1991**, *95*, 8337.
(12) Coolbaugh, M. T.; Whitney, S. G.; Vaidyanathan, G.; Garvey, J. F. *J. Phys. Chem.* **1992**, *96*, 9139.
(13) Castelman, A. W., Jr.; Guo, B. C. *J. Am. Chem. Soc.* **1992**, *114*, 6152.
(14) Brodbelt, J. S.; Liou, C. C.; Maleknia, S.; Lin, T. J.; Lagow, R. J. *J. Am. Chem. Soc.* **1993**, *115*, 11069.
(15) Daly, G. M.; El-Shall, M. S. *Z. Phys. D* **1993**, *26*, S186.
(16) Daly, G. M.; El-Shall, M. S. *J. Phys. Chem.* **1994**, *98*, 696.
(17) Daly, G. M.; El-Shall, M. S. *J. Phys. Chem.* **1995**, *99*, 5283.
(18) Desai, S. R.; Feigerle, C. S.; Miller J. *J. Phys. Chem.* **1995**, *99*, 1786.
(19) Daly, G. M.; Pithawalla, Y. B.; Yu, Z.; El-Shall, M. S. *Chem. Phys. Lett.* **1995**, *237*, 97.
(20) Meot-Ner (Mautner), M.; Sieck, L. W.; El-Shall, M. S.; Daly, G. M. *J. Am. Chem. Soc.* **1995**, *117*, 7737.
(21) El-Shall, M. S.; Daly, G. M.; Yu, Z.; Meot-Ner (Mautner), M. *J. Am. Chem. Soc.* **1995**, *117*, 7744. El-Shall, M. S. *Polym. Prepr.* **1996**, *37*, 367.

S0002-7863(96)02635-2 CCC: $14.00

technique for bulk polymerization by the impact of metal atoms and ions on the liquid monomer.[6,8]

The present olefin condensation process is initiated by charge transfer from an aromatic center which is ionized selectively in a complex mixture, using resonant two-photon ionization[22] high-pressure mass spectrometry (R2PI-HPMS).[23] The ionized aromatic center can bind to an olefin molecule and induce on it a positive charge density sufficient for nucleophilic attack by a second olefin molecule. These reactions belong to the so far small class of higher-order ion−molecule reactions where an ion associates with a molecule and activates it for reaction with a further molecule. Examples are the reactions of O_3, N_2O_5, and NO_2 adsorbed on alkali metal cations,[24,25] ion-assisted reactions of HCl with $ClONO_2$,[26] and reactions of silicon atoms clustered to naphthalene$^+$.[27] In particular, the present reactions are similar to the dimerization of the fluorinated olefin C_2F_4 to form C_4F_8 through association with and then elimination of CF_3^+,[28] but in the present case, the ion also serves as a charge donor. There is also a basic analogy with reactions of a hydrocarbon ion and two H_2O molecules[29] or an ionized aromatic and two polar molecules[23] to form protonated dimers, where neutrals attached to the ion react with an additional molecule to extract a proton from the hydrocarbon ion. In these systems proton transfer to one polar molecule would be endothermic and is not observed, but reactions with two molecules are driven energetically by the formation of a strong hydrogen bond of 30 kcal/mol to form a protonated dimer. The present system is basically similar, but it results in covalent, rather than hydrogen, bond formation. In the present system the aromatic core ion serves as both an activator and a charge donor, similar to an anode in electrochemical polymerization.[30]

The present system constitutes an extension of our studies of polymerization in isobutene.[20,21] In our first studies, polymerization was initiated by a full charge on the *i*-$C_4H_8^{\bullet+}$ reactant, or by partial charge transfer to the olefin in the $[C_6H_6 \cdot i\text{-}C_4H_8]^{\bullet+}$ complex. The ionization potentials (IPs) of the components in this complex are similar within 0.1 eV, and therefore a charge density of about 0.5 may be located on the olefin, which is apparently still sufficient for activating the olefin.

A basic question arises as to how much charge density on a molecule is still sufficient to activate it to undergo ionic type process. The charge density can be varied in aromatic−olefin systems with various differential IPs of the components, leading to various degrees of charge distribution between the reactants. In this paper we shall investigate several systems with varying IP differences.

Experimental Section

The application of R2PI-HPMS has been described in detail elsewhere.[23] Briefly, the HPMS ion source is a cubic aluminum block of about 2 cm^3, fitted with quartz windows through which the laser beam enters and exits. The source is placed inside a vacuum chamber which is also equipped with windows. The cell temperature is monitored through two type T copper−constantan thermocouples (Omega). Gas mixtures are prepared in a heated (>100 °C) 2 L flask and admitted to the ion source at selected pressures via an adjustable needle valve. The cell pressure is monitored with a 0.01−10 Torr capacitance manometer (MKS, 1301) coupled with the gas inlet tube. Mixtures are typically made by microliter injection of liquid samples into the evacuated heated sample flask followed by the addition of the bath gas (Ar in the present study).

In the isobutene/toluene system, the R2PI of toluene was obtained via the 0^0_0 transition at $\lambda = 266.76$ nm. We also used two-photon ionization at $\lambda = 258.94$ nm, and the results were similar to those obtained using the 0^0_0 resonance ionization. These photons create C_6H_5-$CH_3^{\bullet+}$ ions with excess energy of 0.48 or 0.74 eV, respectively, above the IP, much lower than the excess energy required for ring opening in ionized benzene, 3.5−5.0 eV.[31−33]

The laser beam is slightly focused within the center of the cell using a quartz spherical lens ($f = 60$ cm, $d = 2.54$ cm). The laser output ($\lambda = 266.76$ nm, 100−300 μJ, $\Delta t = 15$ ns, 10 Hz repetition rate) is generated by an excimer (XeCl) pumped dye laser (Lambda Physik LPX 101 and FL-3002, respectively). Coumarin 540A (Exciton) dye laser output passes through a β-BaB_2O_4 crystal (CSK) cut at 52° to generate tunable frequency-doubled output of 10^{-8} s pulses. The spatially filtered ultraviolet radiation passes through the high-pressure cell, and focusing is adjusted to minimize three photon processes (i.e., unimolecular fragmentation) while still providing sufficient ion current (photon power density $\sim 10^5$ W/cm^2). The reactant and product ions escape through a precision pinhole (200 μm, Melles Griot) and are analyzed with a quadrupole mass filter.

The quadrupole mass filter (Extrel C-50, equipped with 1.9 cm diameter rods having a resolution better than 1 amu, FWHM, in the mass range of 1−500 amu) is mounted coaxially to the ion exit hole. The distance from the ion exit hole to the C50 lens stack is approximately 2 cm. The ion current from the electron multiplier is amplified and then recorded with a 350 MHz digital oscilloscope (LeCroy 9450).

Ion signal intensities of each ion were integrated for 40−80 s to obtain sufficient signal intensity. The main source of error in the measurements was possible drift in the signal intensities while all the ions were recorded. To check and minimize this effect, each ion intensity was recorded in ascending mass order and then recorded again proceeding in reverse order. The replicate measurements were compared, and the experiment was accepted only if intensities in the replicate measurements for all ions differed by <15%. In the acceptable experiments, the signal intensities from the replicate measurements were summed and averaged. When measured in this manner, relative ion intensities obtained in 4−6 replicate experiments were reproducible within ±20%, and rate coefficients (see below) were reproducible within ±30%.

Results

Reaction System. Time-resolved ion profiles are illustrated in Figure 1a, and the normalized intensities are shown in Figure 1b. All ion profile measurements were replicated 2−6 times and yielded relative ion intensities reproducible within ±15%. The main process is the decay of the reactant $C_6H_5CH_3^{\bullet+}$ (i.e., $T^{\bullet+}$) ion and the formation of the dimer ion of *m/z* 112, i.e., $C_8H_{16}^{\bullet+}$, which can also be denoted as *i*-$C_4H_8^{\bullet+}$(*i*-C_4H_8) or $I_2^{\bullet+}$. In parallel, the adduct at *m/z* 148 is also formed. This adduct can be a noncovalent π complex denoted as $C_6H_5CH_3^{\bullet+}$(*i*-C_4H_8) or $T^{\bullet+}$(I), or a covalent adduct *tert*-butyltoluene$^{\bullet+}$, i.e., $CH_3C_6H_4$-*t*-$C_4H_9^{\bullet+}$, denoted as $TI^{\bullet+}$. This is the most stable adduct isomer, and the observed, nonreactive *m/z* 148 ion (and its adducts with *i*-C_4H_8 molecules) probably corresponds to this covalent adduct.

(22) Lubman, D. M.; Li, L.; Hager, J. W.; Wallace, S. C. In *"Lasers and Mass Spectrometry*; Lubman, D. M., Ed.; Oxford University Press: Oxford, 1990.
(23) Daly, G. M.; Meot-Ner (Mautner), M.; Pithawalla, Y. B.; El-Shall, M. S. *J. Chem. Phys.* **1996**, *104*, 7965.
(24) Rowe, B. R.; Viggiano, A. A.; Fehsenfeld, F. C.; Fahey, D. W.; Ferguson, E. E. *J. Chem. Phys.* **1982**, *76*, 742. Viggiano, A. A.; Deakyne, C. A.; Dale, F.; Paulson, J. F. *J. Chem. Phys.* **1987**, *87*, 6544.
(25) Viggiano, A. A.; Deakyne, C. A.; Dale, F.; Paulson, J. F. *J. Chem. Phys.* **1987**, *87*, 6544.
(26) Van Doren, J. M.; Viggiano, A. A.; Morris, R. A. *J. Am. Chem. Soc.* **1994**, *116*, 6957.
(27) Bohme, D. K. *Chem. Rev.* **1992**, *92*, 1478.
(28) Morris, R. A.; Viggiano, A. A.; Paulson, J. F. *J. Phys. Chem.* **1993**, *97*, 6208.
(29) Sieck, L. W.; Searles, S. K. *J. Chem. Phys.* **1970**, *53*, 2601.
(30) Bhadani, S. N.; Parravano, G. In *Organic Electrochemistry;* Beizer, M. M., and Lund, H., Eds.; Marcel Dekker: New York, 1983, p 995.
(31) Jones, E. G.; Bhattacharya, A. K.; Tiernan, T. O. *Int. J. Mass Spectrom. Ion Phys.* **1975**, *14*, 147.
(32) Rosenstock, H. M.; Larkins, J. T.; Walker, J. A. *Int. J. Mass Spectrom. Ion Phys.* **1973**, *11*, 309.
(33) Beynon, J. A.; Hopkinson, J. A.; Lester, G. R. *Int. J. Mass Spectrom. Ion Phys.* **1969**, *2*, 291.

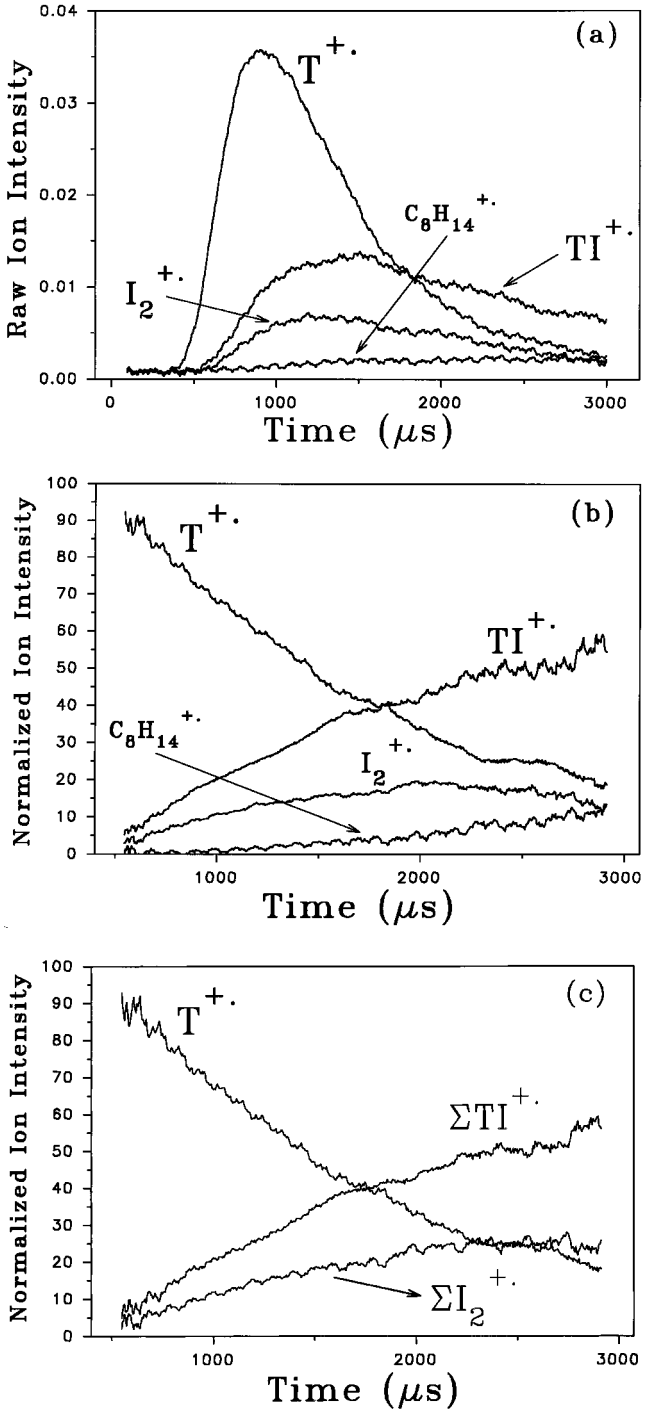

Figure 1. (a) Ion time profiles in the toluene (T)/isobutene (I) system with $P(C_6H_5CH_3) = 0.0052$ Torr ($N = 1.7 \times 10^{13}$ cm^{-3}), $P(i\text{-}C_4H_8) = 0.00083$ Torr ($N = 2.7 \times 10^{13}$ cm^{-3}), and $P(Ar) = 0.71$ Torr ($N = 2.3 \times 10^{16}$ cm^{-3}) at 298 K. Note the parallel formation of $I_2^{\bullet+}$ (*m/z* 112) and $TI^{\bullet+}$ (*m/z* 148) followed by $C_8H_{14}^{\bullet+}$ (*m/z* 110) through a H_2 loss reaction (see ref 20). (b) Normalized intensities of the primary ions. (c) Normalized intensities, with consecutive products from the primary ions $[TI^{\bullet+} + TI_2^{\bullet+}]$ and $[I_2^{\bullet+} + C_8H_{14}^{\bullet+} + I_3^{\bullet+}]$ summed to show the distribution into the primary channels.

Significantly, the formation of the monomer ion $i\text{-}C_4H_8^{\bullet+}$ is not observed. At later reaction times the $C_8H_{16}^{\bullet+}$ ion reacts with $i\text{-}C_4H_8$ to yield the unreactive ion $C_8H_{14}^{\bullet+}$ through H_2 transfer.[20] At long reaction times and high $i\text{-}C_4H_8$ concentrations, small intensities of higher adducts of $i\text{-}C_4H_8$ molecules to the product ions are also observed. In Figure 1c, the intensities of the two products $I_2^{\bullet+}$ and $TI^{\bullet+}$ are summed with their respective further products, i.e., $\sum I_2^{\bullet+} = I_2^{\bullet+} + C_8H_{14}^{\bullet+} + I_3^{\bullet+} + ...$ and $\sum TI^{\bullet+} = TI^{\bullet+} + TI_2^{\bullet+} + ...$, to clearly observe the parallel formation of the primary products.

In several experiments, the $\sum TI^{\bullet+}$ product group continued to increase while the $\sum I_2^{\bullet+}$ product group leveled off after the decay of about 70% of the $T^{\bullet+}$ reactant ion, as observed in Figure 1c after about 2.4 ms. This could indicate reactions into the two product channels from two different isomers of $T^{\bullet+}$. However, the low energy photoionization should not form isomers, as noted above. Also, we observe below that the product distributions into the two channels vary with the concentration of isobutene, which cannot affect the photoproduction of various $T^{\bullet+}$ isomers.

At high laser fluences we observed toluene fragment ions at *m/z* 65^+ and 91^+ and the *tert*-butyl cation (*m/z* 57), and their adducts with $i\text{-}C_4H_8$ molecules. There are no plausible cross-reactions from these even-electron ions to the radical ions of interest, and in fact their summed normalized intensities remain constant with reaction time. Most studies were performed at laser fluences where these ions were negligible, and they are not considered further.

The normalized ion intensities are used to calculate rate coefficients as follows. The pseudo-first-order rate coefficient for the overall reaction $T^{\bullet+}$ to products is calculated from the decay of the reactant ion:

$$k = -\mathrm{d} \ln [T^{\bullet+}]/\mathrm{d}t \qquad (2)$$

The corresponding nominal second-order rate coefficient for the overall forward reaction, k_f, is calculated using the number density of the reactant I as

$$k_f = k/[I] \qquad (3)$$

The nominal second-order rate coefficients for the two channels are calculated from the product distributions as

$$k_f(I_2^{\bullet+}) = k_f[(\sum I_2^{\bullet+})/(\sum I_2^{\bullet+} + \sum TI^{\bullet+})] \qquad (4)$$

$$k_f(TI^{\bullet+}) = k_f[(\sum TI^{\bullet+})/(\sum I_2^{\bullet+} + \sum TI^{\bullet+})] \qquad (5)$$

Rate coefficient measurements were replicated 2−6 times and were reproducible within ±30%. The results are presented in Table 1.

Kinetic Observations. The principal kinetic observations can be summarized as follows.

(1) The overall reaction leading from $T^{\bullet+}$ to $I_2^{\bullet+}$ proceeds orders of magnitude faster than expected for direct endothermic charge transfer ($\Delta H^\circ = +0.42$ eV) from $T^{\bullet+}$ to produce the monomer ion $I^{\bullet+}$ (observed nominal second-order rate coefficients $k = (5-25) \times 10^{-12}$ cm^3 s^{-1} vs expected $k_f \leq k_{collision} \exp(-\Delta H^\circ/RT) \approx 10^{-17}$ cm^{-3} s^{-1}). Analogous and somewhat larger rate enhancement is observed in the benzene/propene system for propene$_2^{\bullet+}$ formation ($\Delta H^\circ = +0.48$ eV, k(obsd) = $(1-5) \times 10^{-12}$ cm^3 s^{-1}, k(expected) ≤ 10^{-18} cm^3 s^{-1}). *In fact, the monomer olefin ions isobutene$^{\bullet+}$ and propene$^{\bullet+}$ are not observed, and the dimer ions appear to form directly through the reactions of the aromatic ions.*

(2) The adduct $TI^{\bullet+}$ and the dimer $I_2^{\bullet+}$ are formed in parallel in comparable yields (Figure 1c), *although the third-body [Ar] or the efficient third-body [C_3H_8], which could collisionally stabilize an excited complex to produce TI$^{\bullet+}$*, are in excess by factors of 200−1000 over the reactant [I] that produces $I_2^{\bullet+}$.

(3) The overall nominal second-order rate coefficient k_f increases with [Ar] (Figure 2), while the product ratio $I_2^{\bullet+}/TI^{\bullet+}$ is independent of [Ar] (Figure 3a). As a result, the nominal

Table 1. Thermochemistry[a] and Kinetics[b] for the Formation of Olefin Dimer Ions B_2^+, Covalent Adducts AB^+,[a] and Neutral Olefin Dimers B_2 in the Reactions of Aromatic Ions A^+ with Olefin B

			$B_2^{+\,b}$		$AB^{+\,c}$		$B_2^{\,d}$		
A^+	B	ΔIP^a	$-\Delta H°^a$	$k_2{}^a$	$k_3{}^a$	$-\Delta H°^a$	$k_2{}^a$	$k_3{}^a$	$-\Delta H°^a$
$C_6H_6^+$	*i*-C_4H_8	0.0	26.2	r[e]		33.7			17.0
$C_6H_5CH_3^+$	*i*-C_4H_8	0.30	16.3[f]	13[f]	5.6[f]	33.5[f]	15[f]	6.6[f]	17.0
				2.0[g]	1.0[g]		4.8[g]	2.5[g]	
$C_6H_6^+$	C_3H_6	0.48	48.7[h]	2.5[h]		36.0[h]	0.81[h]		26.2
1,4-$C_6H_4(CH_3)_2^+$	*i*-C_4H_8	0.80	7.6	nr[i]					17.0
$C_6H_5CH_3^+$	C_3H_6	0.91	38.8	nr[i]		36.0			26.2
$C_6H_6^+$	C_2H_4	1.27	31.2	nr[i]		36.2			27.9

[a] Units: ΔIP, eV; $\Delta H°$, kcal/mol; k_2, 10^{-12} cm^3 s^{-1}; k_3, 10^{-28} cm^6 s^{-1}. Values of k_3 calculated from $k_2 = k_3$[Ar]. Error estimates for rate coefficients, based on replicate measurements, ±30%. [b] Thermochemistry for the reactions $A^{\bullet+} + 2B \rightarrow B_2^{\bullet+} + A$, with the formation of (*E*)-$CH_3CHCHCH_3^{\bullet+}$, $CH_3CHCH_2CH_2CHCH_3^{\bullet+}$, and (*E*)-$(CH_3)_2CHCHCHCH(CH_3)_2^{\bullet+}$ as plausible condensation products for the ethylene, propene, and isobutene dimer cations, respectively.[39] [c] Thermochemistry for the formation of covalent adducts $AB^{\bullet+}$ (benzene/isobutene, toluene/isobutene, benzene/propene, toluene/propene, and benzene/ethylene) is calculated for the products C_6H_5-*t*-$C_4H_9^{\bullet+}$, 1,4-$CH_3C_6H_4$(*t*-$C_4H_9)^{\bullet+}$, C_6H_5-*i*-$C_3H_7^{\bullet+}$, 1,4-$CH_3C_6H_4$(*i*-$C_3H_7)^{\bullet+}$, and $C_6H_5C_2H_5^{\bullet+}$, respectively.[39] [d] Thermochemistry for the reactions $A^{\bullet+} + 2B \rightarrow A^{\bullet+} + B_2$, with formation of the neutral analogues of the isomers in the footnote *b*. [e] Reaction suggested by kinetic simulations (ref 20). [f] Nominal rate coefficients obtained in a reaction system of $P(C_6H_5CH_3) = 0.0010$ Torr ($N = 3.2 \times 10^{13}$ cm^{-3}), P(*i*-C_4H_8) = 0.0016 Torr ($N = 5.2 \times 10^{13}$ cm^{-3}), and P(Ar) = 0.69 Torr ($N = 2.2 \times 10^{16}$ cm^{-3}) at 300 K. The overall nominal forward rate coefficient $k_f{}^2$ was 28×10^{-12}, and the $I_2^{\bullet+}/TI^{\bullet+}$ product ratio was 0.86. For the $I_2^{\bullet+}$ channel, the fourth-order rate coefficient of k_3/[I] = 11×10^{-42} cm^9 s^{-1} applies. [g] Nominal rate coefficients obtained in a reaction system of $P(C_6H_5CH_3) = 0.0010$ Torr ($N = 2.8 \times 10^{13}$ cm^{-3}), P(*i*-C_4H_8) = 0.0018 Torr ($N = 5.1 \times 10^{13}$ cm^{-3}), and P(Ar) = 0.69 Torr ($N = 1.9 \times 10^{16}$ cm^{-3}) at 346 K. The nominal second-order rate coefficient was 6.8×10^{-12} cm^3 s^{-1}, and the product ratio $I_2^{\bullet+}/TI^{\bullet+}$ was 0.42. For the $I_2^{\bullet+}$ channel, the fourth-order rate coefficient of k_3/[I] = 2.0×10^{-42} cm^9 s^{-1} applies. The measurements were done at about constant [Ar] and [I], and the third-order and fourth-order rate coefficients will give similar temperature coefficients. The temperature study was replicated at isobutene number densities of 1.8×10^{13} and 6.9×10^{13} cm^{-3}, and gave similar temperature coefficients. [h] Nominal rate coefficients obtained in a reaction system of $P(C_6H_6) = 0.00068$ Torr ($N = 2.2 \times 10^{13}$ cm^{-3}), $P(C_3H_6) = 0.01$ Torr ($N = 3.2 \times 10^{14}$ cm^{-3}), and P(Ar) = 0.80 Torr ($N = 2.6 \times 10^{16}$ cm^{-3}) at 300 K. [i] nr denotes non-reactive systems, with $k_2 < 10^{-13}$cm^3 s^{-1}.

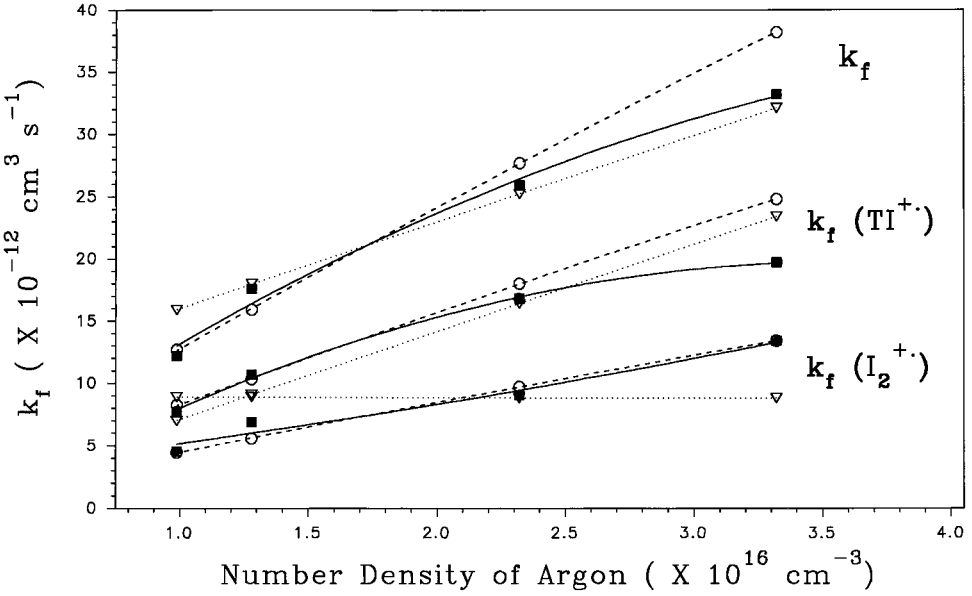

Figure 2. Nominal second-order rate coefficients (10^{-12} cm^3 s^{-1}) as a function of third-body [Ar] number density. Data measured at a constant *i*-C_4H_8 partial pressure of 0.00084 ± 0.00003 Torr (N = $(27 \pm 1) \times 10^{12}$ cm^{-3}) at 298 K. Solid lines are fitted through experimental points (solid squares), broken lines from kinetic simulation of Scheme 1 (open circles), and dotted lines from kinetic simulation of mechanism 2 (open triangles).

second-order rate coefficient $k_f(I_2^{\bullet+})$ for the $I_2^{\bullet+}$ channel and k_f ($TI^{\bullet+}$) for the $TI^{\bullet+}$ channel both increase with [Ar] (Figure 2). The same trends are observed in substituting [Ar] by the efficient polyatomic third-body [C_3H_8] (see Appendix 2). *This is unusual in competitive association/transfer kinetics where the association product usually increases relative to the transfer product with third-body pressure and efficiency.*

(4) The product ratio $I_2^{\bullet+}/TI^{\bullet+}$ increases with [I] (Figure 3b). The nominal second-order rate coefficient $k_f(I_2^{\bullet+})$ for the formation of $I_2^{\bullet+}$ also increases with [I], showing a kinetic order intermediate between [I] and $[I]^2$ dependence (Figure 4).

(5) The products $I_2^{\bullet+}$ (including its higher adducts and $C_8H_{14}^{\bullet+}$) and $TI^{\bullet+}$ (including its higher adducts) do not interconvert, even at high isobutene concentrations (Figure 5).

(6) Toluene concentration has no significant effect on the rate coefficients and product distributions (Figure 6).

(7) With decreasing temperature, the rate of the reaction into both channels increases sharply, and the $I_2^{\bullet+}/TI^{\bullet+}$ product ratio increases (Table 1).

(8) In the reactive systems, the rate coefficients vary inversely with ΔIP (Table 1). Olefin dimer ions are formed in reaction systems with $\Delta IP \leq 0.42$ eV, and not formed for $\Delta IP \geq 0.87$ eV between the components. Decreasing dimer formation with increasing ΔIP is observed also in preformed clusters.[34]

Discussion

Reaction Mechanism. In this section we shall show that the kinetic features are consistent with a mechanism that involves an additional complex along the reaction pathway, subsequent to the usual excited complex. Kinetic considerations

(34) El-Shall, M. S.; Yu, Z. *J. Am. Chem. Soc.* **1996**, *51*, 13058.

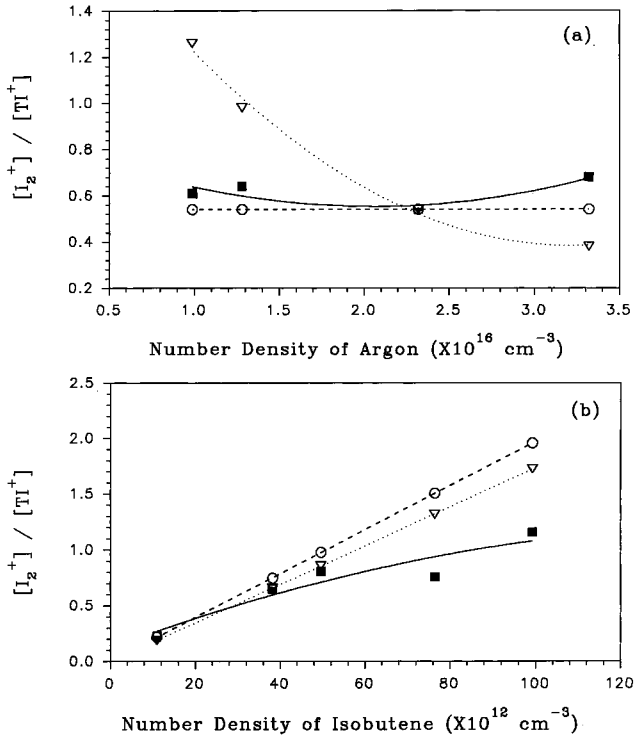

Figure 3. Product distribution ratio $[I_2^{\bullet+}]/[TI^{\bullet+}]$ (a) as a function of third-body number density, measured under the conditions given in the Figure 2 caption and (b) as a function of *i*-C_4H_8 number density. Data measured at constant total pressure of 0.80 Torr ($N = 2.6 \times 10^{16}$ cm^{-3}) at 298 K. Solid lines are fitted through experimental points (solid squares), broken lines from kinetic simulation of Scheme 1 (open circles), and dotted lines from kinetic simulation of mechanism 2 (open triangles).

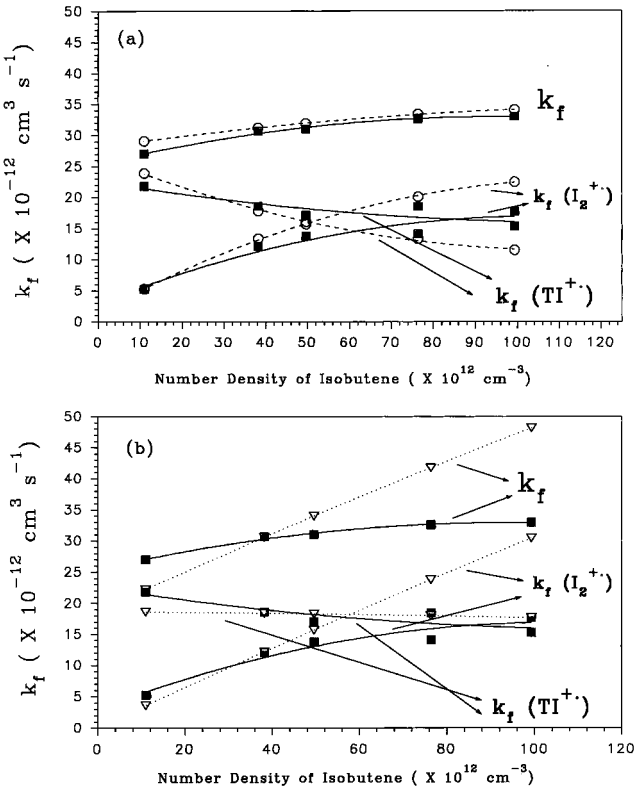

Figure 4. Nominal second-order rate coefficients (10^{-12} cm^3 s^{-1}) as a function of *i*-C_4H_8 number density. Data measured at a constant source pressure of 0.80 Torr ($N = 2.6 \times 10^{16}$ cm^{-3}). (a) Solid lines are fitted through experimental points (solid squares) and broken lines from kinetic simulation of Scheme 1 (open circles). (b) Solid lines are fitted through experimental points and dotted lines from kinetic simulations of mechanism 2 (open triangles). (See Appendix 1b.)

concerning more simple alternative mechanisms are presented below and in Appendix 1. The proposed mechanism is summarized in Scheme 1(mechanism 1) (reactions 6−9).

Scheme 1

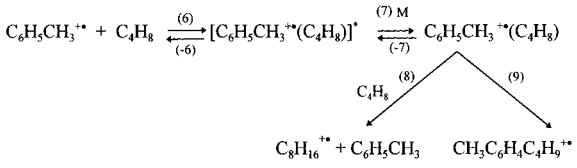

Note that the mechanism involves three different adducts between $C_6H_5CH_3^{\bullet+}$ and *i*-C_4H_8. The existence of these complexes is inferred from the kinetic observations; of course, they all correspond to *m/z* 148, and are indistinguishable mass spectrometrically. In Scheme 1, the excited complex $[C_6H_5CH_3^{\bullet+}(C_4H_8)]^*$, i.e., $[T^{\bullet+}(I)]^*$, is formed in reaction 6, and it undergoes stabilization to the noncovalent complex $C_6H_5CH_3^{\bullet+}(C_4H_8)$, i.e., $T^{\bullet+}(I)$, by collisional or radiative stabilization (reaction 7). The complex then isomerizes to the final, presumably covalent adduct $CH_3C_6H_4$-*t*-$C_4H_9^{\bullet+}$, i.e., $TI^{\bullet+}$ (reaction 9). In a competitive process, the stabilized noncovalent $T^{\bullet+}(I)$ adduct also reacts with I to form $I_2^{\bullet+}$, presumably through an intermediate complex $C_6H_5CH_3^{\bullet+}(C_4H_8)_2$ (reaction 8).

Assuming that the formation of the stabilized noncovalent $T^{\bullet+}(I)$ is rate-controlling for the overall forward reaction, we obtain

$$k_f = k_6(k_7[M] + k_{7r})/(k_{-6} + k_7[M] + k_{7r}) \qquad (10)$$

Here $k_7[M]$ is the rate of collisional stabilization and k_{7r} is the rate of radiative stabilization. If $k_{-6} \gg k_7[M] + k_{7r}$, as indicated

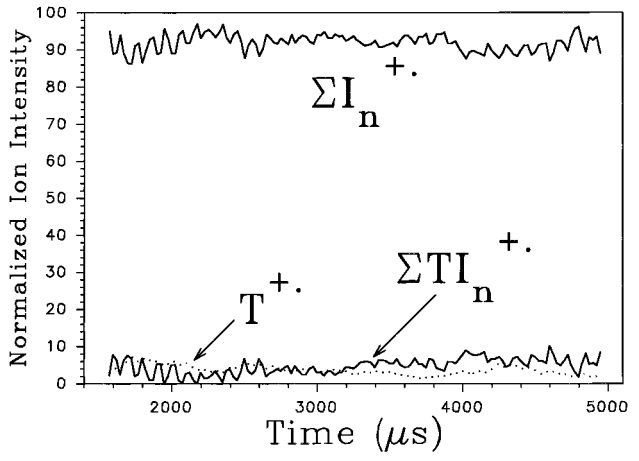

Figure 5. Normalized ion time profiles in the toluene/isobutene system at 298 K, at high *i*-C_4H_8 concentration, showing the absence of interconversion between the products $I_n^{\bullet+}$ and $TI_n^{\bullet+}$ at high isobutene concentration. $P(C_6H_5CH_3) = 0.00062$ Torr ($N = 2.0 \times 10^{13}$ cm^{-3}), P(*i*-C_4H_8) = 0.023 Torr ($N = 7.5 \times 10^{14}$ cm^{-3}), and P(Ar) = 1.0 Torr ($N = 3.2 \times 10^{16}$ cm^{-3}) at 298 K.

by the small overall efficiency, then

$$k_f = k_6(k_7[M] + k_{7r})/k_{-6} \qquad (11a)$$

With respect to the contributions of collisional and radiative stabilization, i.e., $k_7[M]$ vs k_{7r}, we note that k_f is proportional to the third-body density as observed in Figure 2, suggesting that collisional stabilization is dominant under high-pressure conditions. We note however that the intercept of k_f vs [Ar] is not at the origin. Therefore, radiative stabilization may contribute

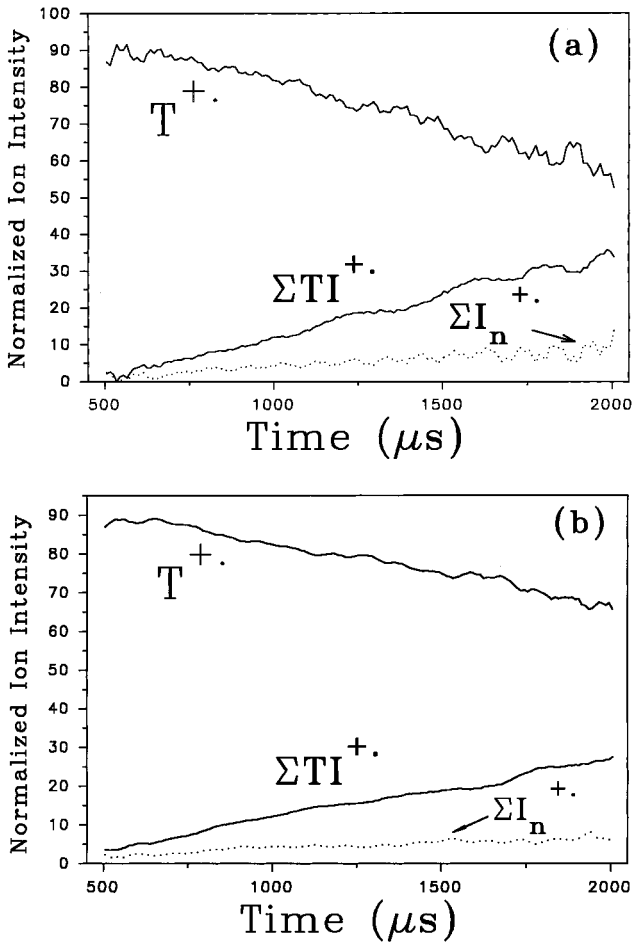

Figure 6. Normalized ion time profiles in the toluene/isobutene system at low and high $C_6H_5CH_3$ concentration, demonstrating the absence of significant effects on the ion time profiles. (a) $P(C_6H_5CH_3) = 0.00015$ Torr ($N = 4.9 \times 10^{12}$ cm^{-3}), $P(i\text{-}C_4H_8) = 0.00035$ Torr ($N = 1.1 \times 10^{13}$ cm^{-3}), $P(\text{Ar}) = 0.72$ Torr ($N = 2.3 \times 10^{16}$ cm^{-3}). (b) $P(C_6H_5CH_3) = 0.0056$ Torr ($N = 182.7 \times 10^{12}$ cm^{-3}), $P(i\text{-}C_4H_8) = 0.00068$ Torr ($N = 22 \times 10^{12}$ cm^{-3}), $P(\text{Ar}) = 0.72$ Torr ($N = 2.4 \times 10^{16}$ cm^{-3}) at 298 K. In the latter system, $(C_6H_5CH_3)_2^{\bullet+}$ is also present (about 20% of the $C_6H_5CH_3^{\bullet+}$ signal intensity), which comes to equilibrium with $C_6H_5CH_3^{\bullet+}$.

significantly at low pressures, as may be expected for these large species with many vibrational modes. Substituting an intercept of $k_f = 10^{-12}$ cm^3 s^{-1} at [M] = 0, and using the other rate coefficients as described in Appendix 2a, yields $k_{7r} = 1.4 \times 10^4$ s^{-1}, about an order of magnitude smaller than the rate of collisions with the third body. However, radiative stabilization may become dominant in low-pressure experiments such as ion cyclotron resonance at $k_{\text{collision}}[\text{M}] < 10^3$ s^{-1}, and such experiments would be of interest.

Under high-pressure conditions where $k_7[\text{M}] > k_{7r}$, eq 11a reduces to eq 11b, and k_f increases with third-body density [M], as is observed in Figure 2.

$$k_f = k_6k_7[\text{M}]/k_{-6} \tag{11b}$$

Assuming that the rearrangement of the stabilized noncovalent intermediate $T^{\bullet+}(I)$ to the final covalent adduct $TI^{\bullet+}$ (reaction 9) is a unimolecular reaction at the high-pressure limit (i.e., pseudo-first-order), then the product ratio will be given by eq 12. The product ratio is then independent of [M], consistent

$$I_2^{\bullet+}/TI^{\bullet+} = k_8[\text{I}]/k_9 \tag{12}$$

with the observation in Figure 3a, and increases with [I], consistent with the observation in Figure 3b. Note that at high [I], the relation becomes nonlinear (Figure 3b), possibly due to excess $TI^{\bullet+}$ production by direct collisions of $[T^{\bullet+}(I)]^*$ with I. The *i*-C_4H_8 molecule can serve as an efficient third body that could stabilize and isomerize the complex directly to the covalent adduct $TI^{\bullet+}$, bypassing the noncovalent adduct $T^{\bullet+}(I)$ (note that reaction 8 requires this adduct).

From Figures 2 and 4, it is evident that the nominal second-order rate coefficients k_f, $k_f(I_2^{\bullet+})$, and $k_f(TI^{\bullet+})$ are actually composite entities of a complex *k*inetic order with respect to [I] and [Ar]. Note that k_f is a second-order rate coefficient obtained using eq 3, i.e., $k_f = k/[\text{I}]$. Figure 2 shows that at low third-body density k_f is also proportional to [Ar], and the pseudo-first-order overall rate coefficient is therefore proportional to [I][Ar]; i.e., the overall reaction is third-order. Third-order rate coefficients are reported in Table 1.

Figure 4 shows that, at low [I], the nominal second-order rate coefficient $k_f(I_2^{\bullet+})$ calculated from eqs 2−4 is proportional to [I], and therefore the pseudo-first-order rate of the reaction to produce $I_2^{\bullet+}$ is proportional to $[\text{I}]^2$. From Figure 2, it is also proportional to [Ar] at low third-body densities. Therefore, at low [I] and [Ar], the pseudo-first-order rate varies as $[\text{I}]^2[\text{Ar}]$ and the rate coefficients for the formation of $I_2^{\bullet+}$ are fourth-order with values of 11×10^{-42} cm^9 s^{-1} at 300 K and 2×10^{-42} cm^9 s^{-1} at 346 K.

To further test the mechanism, we simulated Scheme 1 using the ACUCHEM program for coupled reactions,[35] using rate coefficients as explained in Appendix 2. The model should be able to reproduce the effects of varying [I] and [Ar] as shown in Figures 2−4.

Figures 2−4 show that the simulations reproduce the observed trends, at least qualitatively. Specifically, Figure 2 shows that the overall rate coefficient k_f increases with [Ar]. Referring to Scheme 1, this is due to increasing competition of the collisional stabilization of $[T^{\bullet+}(I)]^*$ with increasing [Ar], vs back-dissociation. Correspondingly, the rate coefficients for the two products, $k_f(I_2^{\bullet+})$ and $k_f(TI^{\bullet+})$, also increase in parallel and maintain a constant product ratio. In both the experiment and simulations, k_f tends to level off at high [Ar], as its value would ultimately have to become constant when reaching the collision rate.

Figure 3a shows that the product ratio remains constant with [Ar], as $k_8[\text{I}]$ and k_9 are independent of [Ar]. Figure 3b shows that the product ratio increases with [I], as $k_8[\text{I}]/k_9$ increases with [I]. We note a significant deviation toward increased $TI^{\bullet+}$ vs $I_2^{\bullet+}$ production at high [I]. A possible reason could be that $[T^{\bullet+}(I)]^*$ may be isomerized directly to the nonreactive covalent adduct $TI^{\bullet+}$ through collision with the efficient third-body I.

Figure 4 shows that the overall rate coefficient k_f increases slightly with [I]. This results from the more efficient competition of the forward reaction channels of $T^{\bullet+}(I)$ compared with back-dissociation through $(T^{\bullet+}I)^*$ as $k_8[\text{I}]$ increases vs k_{-7}. We also observe the increase of $k_f(I_2^{\bullet+})$ with increasing [I]. Note that at the same time $k_f(TI^{\bullet+})$ decreases, as with increasing k_8-[I] vs constant k_9, the dimer channel competes more effectively. Also note that the simulation reproduces the nonlinear variation of these partial rate coefficients with [I].

Another feature of the simulations is that, with the rate coefficients used, the concentrations of the reactive, noncovalent $[T^{\bullet+}(I)]^*$ and $T^{\bullet+}(I)$ adducts always remain 2−4 orders of magnitude below the sum of the other species, consistent with these species being transient intermediates.

We observe a decrease in the overall rate coefficient with increasing temperature. This can be attributed to the increasing

(35) ACUCHEM Version 1.4, copyright National Institute of Standards and Technology, Nov 7, 1986.

rate coefficient k_{-6} for the back-dissociation exciting the complex $[T^{\bullet+}(I)]^*$, similar to the effect that leads to negative temperature coefficients in ion−molecule association reactions. However, reactions 8 and 9 may involve barriers, and k_8 and k_9 may increase with temperature, leading to complex overall temperature coefficients.

Further support for reaction 8 of a noncovalent adduct is obtained by observations in preformed aromatic/olefin clusters in which the aromatic molecule was selectively photoionized.[21,34] The results show close similarities between the cluster and gas phase studies, as summarized below.

(1) In benzene (B)/isobutene, where the IPs are similar, in both studies $I_2^{\bullet+}$, $BI^{\bullet+}$, and their higher adducts with I are observed. Also observed are $I^{\bullet+}$ and its reaction product with I, i.e., t-$C_4H_9^+$. The results indicate that charge transfer from benzene$^{\bullet+}$ to i-C_4H_8 occurs in both the gas phase and in clusters.[20,21]

(2) In toluene/isobutene, $I_2^{\bullet+}$ and $TI^{\bullet+}$ are observed. However, $I^{\bullet+}$ and its t-$C_4H_9^{\bullet+}$ product are not observed in either the gas phase or clusters, indicating that $I_2^{\bullet+}$ is formed directly in both cases. In all of the reactions observed, the monomer olefin ion and its product, the protonated olefin monomer, are not observed in either phase where the IP of the aromatic is lower than that of the olefin.

(3) In *p*-xylene/isobutene, no $I_2^{\bullet+}$ is observed in the gas phase. It is observed in the clusters, but in very small yield.[34] Spectral shifts in the clusters indicate that $I_2^{\bullet+}$ is formed from larger clusters containing several I molecules, where a cooperative process involving several olefin molecules can effectively lower the IP of the aggregate to allow ultimate charge transfer from the aromatic center.

(4) In benzene/propene, [(propene)$_n^{\bullet+}$, $n \geq 2$] and [benzene$^{\bullet+}$-(propene)$_n$] adducts are observed in both the gas phase and clusters.

(5) Olefin dimers are not observed in toluene/propene and benzene/ethylene, either in the gas phase or in clusters. Also, no $I_2^{\bullet+}$ is observed in the mesitylene/isobutene system in clusters. In other words, in systems where the IP difference between the reactants is >0.87 eV, the olefin dimer ion is not formed in either phase.

The close similarities between the gas phase and the "semi-condensed" cluster phase suggest that the same mechanism is operative in both. This suggests that the mechanism can possibly apply also in the condensed phase. The cluster studies are reported in detail elsewhere.[34]

Reaction Complexes and Products. In a preceding study[20] we observed the formation of $C_8H_{16}^{\bullet+}$ from i-$C_4H_8^{\bullet+}$ + i-C_4H_8. The product was identified as a covalent ion of an octene with an IP of 8.55 ± 0.15 eV, possibly $(CH_3)_2CHCHCHCH(CH_3)_2^{\bullet+}$. It reacted with i-C_4H_8 by H_2 transfer, yielding a nonreactive $C_8H_{14}^{\bullet+}$. The present $C_8H_{16}^{\bullet+}$ ion shows similar chemistry (Figure 1b). We also note that the product ion must correspond to a neutral with an IP < 8.82 eV (the IP of toluene), since otherwise the reaction would more likely produce $C_6H_5CH_3^{\bullet+}$ + C_8H_{16}, amounting to ion-catalyzed dimerization of neutral i-C_4H_8 similar to the reaction of CF_3^+ with two C_2F_4 molecules to produce C_4F_8.[28] These considerations are consistent with a product octene ion branched on the olefinic carbon atom. It is of interest whether the dimer ion formed in the $C_6H_5CH_3^{\bullet+}$-(i-C_4H_8)$_2$ complex is the same as that formed in the reaction of i-$C_4H_8^{\bullet+}$ with i-C_4H_8 in the gas phase.[20]

We observe that the final, presumably covalent, $CH_3C_6H_4$-t-$C_4H_9^{\bullet+}$ adduct does not interconvert to form the isobutene dimer $C_8H_{16}^{\bullet+}$. This suggests that the reactive $C_6H_5CH_3^{\bullet+}$-(i-C_4H_8) adduct may be a noncovalent aromatic/olefin π complex similar to aromatic dimer ions that we investigated previously, which for the present IP difference of 0.42 eV typically have binding energies of 12−15 kcal/mol.[36,37] Alternatively, the complex may be a covalent distonic radical cation similar to those observed by Holman et al. in the reactions of $C_6H_6^{\bullet+}$ with cycloalkanes.[38] These species have higher energies than the π-ionized alkylbenzene cations, and may serve a role similar to that of a noncovalent complex.

For the formation of the nonreactive 1,4-$CH_3C_6H_4$-t-$C_4H_9^{\bullet+}$ covalent adduct, the thermochemistry gives $\Delta H^\circ = -33.5$ kcal/mol.[39] In relation to its possible back-dissociation to C_6H_5-$CH_3^{\bullet+}$ + i-C_4H_8, the observations would yield equilibrium ion ratios of $[TI^{\bullet+}]/[T^{\bullet+}] \geq 100$. In the model reaction system used for Figure 1 this leads to $-\Delta G^\circ$ (300) ≥ 10.5 kcal/mol, and a typical association entropy change of $\Delta S^\circ = -35$ cal/(mol K) gives $-\Delta H^\circ \geq 21$ kcal/mol, consistent with a covalent adduct.

We note that the two distinct isomers, a reactive $C_6H_5CH_3^{\bullet+}$-(i-C_4H_8) complex and the unreactive covalent $CH_3C_6H_4$-t-$C_4H_9^{\bullet+}$ adduct, suggests a barrier between them. This barrier is below the energy of the reactants, since the temperature coefficient for the formation of $CH_3C_6H_4$-t-$C_4H_9^{\bullet+}$ is negative. The barrier for the reaction of $C_6H_5CH_3^{\bullet+}$(i-C_4H_8) with i-C_4H_8 to form $C_8H_{16}^{\bullet+}$ must still be lower, possibly negligible, as indicated by the fact that the temperature coefficient for the formation of $C_8H_{16}^{\bullet+}$ is even more negative.

Other Reaction Systems and the Relation between Reactivity and Energetics. A main point of interest is the charge density on the olefin component in the $A^{+\bullet}$(B) complexes, which depends on the IP difference between the components.[36,37] The question is how large a ΔIP between the components still places enough charge density on the olefin to allow nucleophilic attack by another olefin molecule.

To investigate this question, we examined several aromatic−olefin combinations $A^{\bullet+}$ + B as shown in Table 1. To consider all the possible reactions in these systems, we also present the thermochemistry for the formation of the $AB^{\bullet+}$ adducts, probably alkylbenzene ions, that are observed in all the systems.

Table 1 shows an inverse relation between the ΔIPs of the components and the rate coefficients to form $B_2^{\bullet+}$. As noted above, the formation of $B_2^{\bullet+}$ is observed for reactants with a ΔIP < 0.42 eV, but not for larger ΔIP, even though the formation of $B_2^{\bullet+}$ would always be significantly exothermic.

Hypothetical ion-catalyzed dimerization ($A^{\bullet+}$ + 2B → $A^{\bullet+}$ + B_2) leading to the neutral olefin dimer is also exothermic for all the reaction systems in Table 1. Its energetics are less favorable than for the formation of the ionic olefin $B_2^{\bullet+}$ dimers in most of the systems. Exceptions are the toluene/isobutene system where the energetics are similar and the *p*-xylene/isobutene system in which an ionic dimer is less energetically favored and is in fact not observed in the gas phase. This ion-catalyzed process may in fact be occurring in any of the reaction systems that we investigated, even with high efficiency, but since it does not lead to new ionic products, we would not observe it.

We noted that the ΔIP of 0.48 eV in the benzene/propene system makes direct endothermic charge transfer even more strongly prohibitive than in the toluene/isobutene system, with an expected efficiency of $k/k_{collision} = \exp(-\Delta H^\circ/RT) = 10^{-9}$.

(36) Meot-Ner (Mautner), M.; Hunter, E. P.; Hamlet, P.; Field, F. H. *J. Am. Chem. Soc.* **1978**, *100*, 1466.

(37) Meot-Ner (Mautner), M.; El-Shall, M. S. *J. Am. Chem. Soc.* **1986**, *108*, 4386.

(38) Holman, R. W.; Rozeboom, M. D.; Gross, M. L.; Warner, C. D. *Tetrahedron.* **1986**, *42*, 6235. Holman, R. W.; Warner, C. D.; Hayes, R. N.; Gross, M. L. *J. Am. Chem. Soc.* **1990**, *112*, 3362.

(39) Lias, S. G.; Bartmess, J. E.; Liebman, J. F.; Levin, R. D.; Mallard, W. G. *J. Phys. Chem. Ref. Data* **1988**, *17*, Suppl 1.

Furthermore, the IP of propene, 9.73 eV, is above the two-photon energy used to ionize benzene, 9.58 eV, so that direct charge transfer from excited $(C_6H_6^{\bullet+})^*$ can be ruled out energetically. Therefore, this system presents an energetically even more clear-cut candidate to distinguish between dimer formation through the proposed reaction 8 or through direct charge transfer followed by dimer formation (see Appendix 1a). We have, in fact, confirmed the direct mechanism of the benzene/propene system by an independent method using the selected ion flow tube (SIFT) technique. The mass-selected $C_6H_6^{\bullet+}$ ion was injected into a He/C_3H_6 gas flow (not containing $C_3H_6^{\bullet+}$). The production of $(C_3H_6)_n^{\bullet+}$ ions was observed, with $n = 2-6$, with rate coefficients comparable to those measured in our R2PI-HPMS method. The results will be reported elsewhere.[40]

Summary, and Implications for Industrial and Astrochemical Polymerization

The main observation is a coupled reaction of dimer formation and ionization of the olefin dimer. These processes are observed in simple gas-phase reactions of an ionized aromatic molecule with two olefin molecules. The observed kinetic trends, especially the pressure effects, are best reproduced by a mechanism through a collisionally stabilized noncovalent intermediate complex $A^{\bullet+}(B)$ in which the olefin molecule is "adsorbed" on the ionized aromatic surface, and assumes a charge density by interaction with the aromatic ion. Upon collision with another olefin molecule, in the resulting $A^{\bullet+}(2B)$ complex, one olefin molecule can carry sufficient charge density to activate it for nucleophilic attack by the second olefin molecule, resulting in covalent condensation. Formation of an olefin with a lower IP than that of the aromatic component will then result in full charge transfer, leading to the observed product ion. Alternatively, the required processes in the $A^{\bullet+}(2B)$ complex may occur simultaneously. Other alternative mechanisms are discussed in the Appendices. Theoretical study of the potential energy surfaces and transition states may help to identify the mechanism.

The observed processes add to the small group of multibody ion−molecule reactions where attachment to an ion activates a neutral molecule for reaction with a further neutral molecule.

The observed reactions are similar to anodic electrochemical polymerization, where strong anionic nucleophiles added to olefins were assumed to reduce their effective oxidation potentials,[41] although in the complex solution system this was debated.[42] The present simple gas-phase systems are clearer examples where collaborative interaction between substrate molecules effectively shifts their oxidation potential and allows charge transfer from the "electrode", which is otherwise prohibitively endothermic.

The toluene−isobutene reaction shows a significant negative temperature dependence. The present exploratory two-point study cannot define the functional form which may be complex because of the multistep mechanism and because of nonexponential terms.[43] As an estimate, using $k_f = aT^n$, the second-order rate coefficients for the formation of $I_2^{\bullet+}$ and $TI^{\bullet+}$ would give temperature coefficients as large as $T^{-12.9}$ and $T^{-7.8}$, and extrapolate to the collision rate at 214 and 168 K, respectively. This suggests that the reactions may achieve unit collision efficiency already at moderately low temperatures. At interstellar temperatures below 100 K, such reactions can therefore become effective synthesis pathways. Moreover, at such low temperatures large clusters of monomers can attach to an ionized aromatic and allow concerted multistep polymerization to drive substantially endothermic charge transfer from the aromatic surface. Low temperatures may also be useful in industrial applications. More detailed temperature studies are of interest to define the functional form of the temperature coefficients.

The present mechanism avoids the formation of the olefin monomer ions and their reaction products. For example, in the benzene/propene system we observed the exclusive formation of $(propene)_n^{\bullet+}$ with $n = 2-7$. In contrast, ion−molecule reactions between $C_3H_6^{\bullet+}$ and C_3H_6 produce $C_3H_7^+$, $C_4H_7^+$, $C_4H_8^{\bullet+}$, and $C_5H_9^+$ that can further polymerize.[44,45] The present mechanism leads exclusively to the $C_6H_{12}^{\bullet+}$ radical dimer ion channel, suggesting a useful photoinitiation method for pure products.

We noted the similarity of the gas-phase observations to those in preformed clusters.[34] This suggests that the mechanism may also apply in the condensed phase in common aromatic solvents such as toluene. This can allow photoinitiation using a *"solvent as initiator approach"* to eliminate chemical initiators, with beneficial economic and environmental results.

Acknowledgment. This research is supported by the National Science Foundation (Grant No. CHE 9311643). Acknowledgment is also made to the Thomas F. and Kate Miller Jeffress Memorial Trust (Grant No. J-302) for the partial support of this research.

Appendix 1. Alternative Mechanisms

a. Direct Charge Transfer, Followed by Dimer Formation. This mechanism would entail charge transfer from $T^{\bullet+}$ to I through the dissociation of the reaction complex $T^{\bullet+}(I)^*$ to $I^{\bullet+} + T$, in competition with stabilization to form $TI^{\bullet+}$. We do not observe the formation of $I^{\bullet+}$, but if formed, it could react rapidly with T by charge transfer to form $T^{\bullet+}$ and with I to form $C_8H_{16}^{\bullet+}$ (and t-$C_4H_9^+$). Therefore, its absence in detectable concentrations does not rule out conclusively its formation. However, as noted in observation 1 above, equating the 0.42 eV endothermicity with the activation energy suggests a reaction efficiency $r = k/k_{collision} = \exp(-E_a/RT)$ of 10^{-7}. This calculation is based on relative IPs from evaluated accurate thermochemical data.[46] In comparison, the observed nominal second-order rate coefficient for the formation of $I_2^{\bullet+}$ (and through it, its subsequent products) under the present conditions ranges from 5 to 25 $\times 10^{-12}$ cm^3 s^{-1}. The observed reaction efficiency of $(0.5-2.5) \times 10^{-2}$ is about 5 orders of magnitude larger than expected for direct charge transfer.

Other evidence against the formation of i-$C_4H_8^{\bullet+}$ is the lack of formation of t-$C_4H_9^+$, a known product of the reaction of i-$C_4H_8^{\bullet+}$ with i-C_4H_8 under similar conditions.[20]

Another test of the direct charge transfer mechanism can be performed by using high concentrations of toluene, to use T as a scavenger for $I^{\bullet+}$. In the direct transfer mechanism, the $I^{\bullet+}$ product would react competitively with I to give $I_2^{\bullet+}$ in reaction 8, and with T to regenerate $T^{\bullet+}$ by fast exothermic charge transfer. This competing process would become more significant with increasing [T]/[I] density ratios, and the rate of

(40) Pithawalla, Y. B.; Gao, J.; Meot-Ner (Mautner), M.; Bohme, D. K. El-Shall, M. S. Manuscript in preparation.
(41) Manning, G.; Parker, V. D.; Adams N. R. *J. Am. Chem. Soc.* **1969**, *91*, 4584.
(42) Eberson, L.; Utley, J. H. P. In *Organic Electrochemistry;* Beizer, M. M., Lund, H., Eds., Marcel Dekker: New York, 1983; p 409.
(43) Viggiano, A. A. *J. Chem. Phys.* **1986**, *84*, 244.
(44) Bowers, M. T.; Elleman, D. D.; O'Malley. R. M.; Jennings, K. R. *J. Phys. Chem.* **1970**, *74*, 2583.
(45) Abramson, F. P.; Futrell, J. H. *J. Phys. Chem.* **1968,** *72*, 1994.
(46) Levin, R. D.; Lias, S. G. *Ionization Potential and Appearance Potential Measurements*, 1971−1981; National Bureau of Standards: Washington, DC, 1982.

production of $I_2^{\bullet+}$ would decrease correspondingly. On the other hand, the production of $TI^{\bullet+}$ through collisional stabilization of $(T^{\bullet+}I)^*$ should not be affected by the [T]/[I] concentration ratio. The net effect is that the $I_2^{\bullet+}/TI^{\bullet+}$ product ratio would decrease with increasing [T]/[I] concentration ratio. To test this, we performed two experiments under similar conditions but with [T]/[I] ratios of 0.3 and 8.3, i.e., concentration ratios different by a factor of 25. The $I_2^{\bullet+}/TI^{\bullet+}$ product ratio remained constant at 0.3 ± 0.1 in both experiments as shown in Figure 6. This contraindicates an $I^{\bullet+}$ intermediate that would be trapped by T.

For these reasons, we can rule out direct charge transfer from $T^{\bullet+}$ to I as a significant process in our system.

b. Competitive Reactions of an Excited Complex. The first step in the reaction is the formation of an excited complex $[T^{\bullet+}(I)]^*$. Evidence for its formation and back-dissociation to reactants is the low overall reaction efficiency, $<10^{-2}$.

The common ion−molecule mechanism would proceed through competitive reactions of $[T^{\bullet+}(I)]^*$ by back-dissociation to reactants (reaction −6), in competition with dissociation to products and stabilization, the hypothetical reactions 13−15, that constitute mechanism 2.

$$C_6H_5CH_3^{\bullet+} + C_4H_8 \rightarrow [C_6H_5CH_3^{\bullet+}(C_4H_8)]^* \quad (6)$$

$$[C_6H_5CH_3^{\bullet+}(C_4H_8)]^* \rightarrow C_6H_5CH_3^{\bullet+} + C_4H_8 \quad (-6)$$

$$[C_6H_5CH_3^{\bullet+}(C_4H_8)]^* + M \rightarrow CH_3C_6H_4C_4H_9^{\bullet+} + M \quad (13)$$

$$[C_6H_5CH_3^{\bullet+}(C_4H_8)]^* \rightarrow CH_3C_6H_4C_4H_9^{\bullet+} + h\nu \quad (14)$$

$$[C_6H_5CH_3^{\bullet+}(C_4H_8)]^* + C_4H_8 \rightarrow C_8H_{16}^{\bullet+} + C_6H_5CH_3 \quad (15)$$

Dissociation of $[T^{\bullet+}(I)]^*$ to $I^{\bullet+} + T$ was ruled out in the preceding section, and for a bimolecular process it would have to be replaced by a reaction of $[T^{\bullet+}(I)]^*$ with I to form $I_2^{\bullet+}$. This reaction would bypass the second intermediate $T^{\bullet+}(I)$ in Scheme 1. The formation of the final stable $TI^{\bullet+}$ could be through collisional or radiative stabilization of $[T^{\bullet+}(I)]^*$. Steady-state assumption on $[T^{\bullet+}(I)]^*$ would then yield eqs 16−18 for the formation of the products.

$$k_f^2(I_2^{\bullet+}) = k_6\, k_{15}[I]/(k_{-6} + k_{15}[I] + k_{13}[M] + k_{14}) \quad (16)$$

$$k_f^2(TI^{\bullet+}) = k_6(k_{13}[M] + k_{14})/(k_{-6} + k_{15}[I] + k_{13}[M] + k_{14}) \quad (17a)$$

Assuming radiative stabilization of $[T^{\bullet+}(I)]^*$, i.e., if $k_{14} \gg k_{13}[M]$, then $k_{13}[M]$ would be negligible in the denominator of eq 17a, and the overall forward rate coefficient $k_f = k_f(I_2^{\bullet+}) + k_f(TI^{\bullet+})$ would be independent of third-body density [M], in contrast to the results in Figure 2. The results therefore suggest predominantly collisional stabilization under our high-pressure conditions, although radiative stabilization may be significant at low pressures, as discussed above. Under our conditions $k_{13}[M] \gg k_{14}$ and eq 17a reduces to eq 17b.

$$k_f^2(TI^{\bullet+}) = k_6(k_{13}\,[M])/(k_{-6} + k_{15}[I] + k_{13}[M]) \quad (17b)$$

The product ratio according to this mechanism would be given by eq 18a. With collisional stabilization predominant, i.e., with

$$I_2^{\bullet+}/(TI)^{\bullet+} = k_{15}[I]/(k_{13}[M] + k_{14}) \quad (18a)$$

$k_{13}[M] \gg k_{14}$, eq 18a is reduced to eq 18b.

$$I_2^{\bullet+}/(TI)^{\bullet+} = k_{15}[I]/(k_{13}[M]) \quad (18b)$$

The product ratio $I_2^{\bullet+}/TI^{\bullet+}$ would be inversely dependent on [M], which is contrary to the results in Figure 3a. However, at high pressures of the efficient third-body I, this mechanism may contribute to the formation of $TI^{\bullet+}$, as suggested by the decrease of the $I_2^{\bullet+}/TI^{\bullet+}$ product ratio in Figure 3b.

We also note that the third-body number density [Ar] is in large excess over [I] in our experiments. For example, in the reaction system in Figure 1, it is in excess by a factor of 850, and large ratios between 200 and 1000 apply in all of our experiments. The product distribution could be explained only if the collisional stabilization efficiency of $[T^{+\bullet}(I)]^*$ by [Ar] is smaller by factors of 200−1,000 than the reaction efficiency with I to form $I_2^{\bullet+}$, i.e., with collision efficiency of Ar < 0.005, at least an order of magnitude smaller than usual even for monoatomic third bodies.

To check the third-body effect, we performed an experiment with an efficient polyatomic collisional third body, *n*-C_3H_8, that has many vibrational modes to absorb the internal energy of the complex. We examined reaction systems with [Ar] or $[C_3H_8] = 1.5 \times 10^{16}$ cm^{-3} and $[I] = 2.8 \times 10^{12}$ cm^{-3}. We found that, with Ar, k_f was 22×10^{-12} cm^3 s^{-1}, and, with *n*-C_3H_8, 44×10^{-12} cm^3 s^{-1}. The partial rate coefficients were, with Ar, $k_f(I_2^{\bullet+}) = 5.8 \times 10^{-12}$ cm^3 s^{-1} and $k_f(TI^{\bullet+}) = 17 \times 10^{-12}$ cm^3 s^{-1}, and with C_3H_8, $k_f^2(I_2^{\bullet+}) = 13 \times 10^{-12}$ cm^3 s^{-1} and $k_f(TI^{\bullet+}) = 32 \times 10^{-12}$ cm^3 s^{-1}. Correspondingly, the $I_2^{\bullet+}/TI^{\bullet+}$ product ratio was with Ar 0.35 and with C_3H_8 0.41. Therefore, the rate coefficients increased by about a factor of 2, and since the collision efficiency of C_3H_8 should be near unity, that of Ar is then ≥0.5. Most importantly, the product distribution did not change significantly with the more efficient third body. Therefore, the product ratio cannot be attributed to low collisional efficiency of the third-body Ar to stabilize the excited $[T^{\bullet+}(I)]^*$ complex.

To further examine mechanism 2, we performed ACUCHEM kinetic simulations applied to the model system of Figure 1, as we did above for Scheme 1. Rate coefficients were assigned as described in Appendix 2. The results in Figure 2 show that the mechanism can simulate the observed pressure effects on k_f as well as mechanism 1 (Figure 2), although it does not match well the pressure effect on the partial rate coefficient $k_f(I_2^{\bullet+})$. In this mechanism the rate formation of $I_2^{\bullet+}$ is limited by $k_{collision}$-[I], and because of the much higher number density of [Ar], the product distribution $I_2^{\bullet+}/TI^{\bullet+}$ could be matched only by using an unusually small collision efficiency of 0.0022 for the stabilization of $[T^{\bullet+}(I)]^*$ by Ar. Furthermore, the third-body density effect on the product distribution $I_2^{\bullet+}/TI^{\bullet+}$ from the simulation shows a strong inverse dependence on [Ar] as shown in Figure 3a, as expected from the analytical solution, eq 18b, above.

All of the kinetic evidence therefore suggests that the competitive transfer/association directly from the excited complex $[T^{\bullet+}(I)]^*$ as in mechanism 2 is less compatible with the experimental observations than Scheme 1.

Appendix 2. Rate Coefficients for Kinetic Simulations

We select rate coefficients for Scheme 1 as follows. For reactions 6, 7, and 8 we assume unit collision efficiency and a rate coefficient of 10^{-9} cm^3 s^{-1}, so the rates are given by 10^{-9}[I] s^{-1} for reaction 6 and 10^{-9}[Ar] s^{-1} for reaction 7. Note that the efficiency of Ar may be <1, but the experiments with propane as carrier gas suggest that the efficiency is ≥0.5 for this reaction as discussed above. We adjusted the other rate coefficients to simulate the model system in Figure 1, on the

basis of the following considerations. In the model system, [I] $= 2.74 \times 10^{13}$ cm^{-3}; therefore, we use k_8[I] $= 2.74 \times 10^4$ s^{-1}. The parallel reaction 9 is a first-order or pseudo-first order reaction as discussed above. The value of $k_9 = 5.07 \times 10^4$ s^{-1} reproduces the product distribution of $[I_2^{\bullet+}]/[TI^{\bullet+}] = 0.54$ observed experimentally in the model system.

To assign k_{-7}, we consider the following points. The order of the overall reaction with respect to [I] depends on the relative rates of the reactions of the complex $T^{\bullet+}$(I). If it is in rapid equilibrium with the reactants through reaction -7, the concentration of $T^{\bullet+}$(I) would be proportional to [I], and the overall rate of formation of $I_2^{\bullet+}$ through reaction 8 would make k_f-($I_2^{\bullet+}$) linear with [I] (i.e., the pseudo-first-order rate coefficient for formation of $I_2^{\bullet+}$ would be proportional to [I]^2). On the other hand, if the formation of $T^{\bullet+}$(I) was rate controlling and irreversible, with $k_{-7} \ll k_8$[I] + k_9, then $k_f(I_2^{\bullet+})$ would be independent of [I], (i.e., the pseudo-first-order rate coefficient for the formation of $I_2^{\bullet+}$ would be proportional to [I]). The results in Figure 4 show an intermediate behavior. This suggests that k_{-7} is comparable to k_8[I] and k_9. Therefore, we used $k_{-7} = 2.68 \times 10^4$ s^{-1}. Finally, the overall reaction rate is controlled primarily by the back-dissociation of the first excited complex $[T^{\bullet+}(I)]^*$, and we adjusted this to $k_{-6} = 6.08 \times 10^8$ s^{-1} to fit the ion profiles in the model experimental system. All of the rate coefficients were kept constant in the simulations of pressure and concentration effects.

To select rate coefficients for mechanism 2, we chose rate coefficients to simulate the reaction system described in Figure 1. As for Scheme 1, for k_6 and k_{15} we apply unit collision efficiency. The product ratio $I_2^{\bullet+}/TI^{\bullet+}$ is given by $k_{collision}$[I]/$k_{collision}$[Ar]f, where an efficiency $f = 0.0022$ must be applied to match the observed product distribution. Note that if we assumed that reaction 15 proceeds with collision efficiency <1, the stabilization efficiency f would have to be proportionally even smaller. To match the observed overall rate coefficient k_f, the required value of k_{-6} is 3.0×10^6 s^{-1}. This value is much smaller than for Scheme 1, as there the back-dissociation competes with stabilization at the rate $k_{collision}$[Ar], while in mechanism 2 it competes with the forward reaction determined by $k_{collision}$[I], under conditions where [Ar] $\gg$ [I]. As for Scheme 1, the rate coefficients were kept constant in the simulations of the pressure and concentration effects.

JA962635X